

Validation of the Octamouse for Simultaneous ^{18}F -Fallypride Small-Animal PET Recordings from 8 Mice

Axel Rominger¹, Erik Mille¹, Shanshan Zhang², Guido Böning¹, Stefan Förster¹, Sebastian Nowak¹, Franz Josef Gildehaus¹, Björn Wängler¹, Peter Bartenstein¹, and Paul Cumming¹

¹Department of Nuclear Medicine, Ludwig-Maximilians University, Munich, Germany; and ²Department of Radiobiology and Oncology Research, Uppsala University, Uppsala, Sweden

Data collection in preclinical small-animal PET studies has been hindered by the small number of recordings typically obtained for a single radiosynthesis. Therefore, we tested procedures for obtaining 8 simultaneous small-animal PET recordings from the brains of 8 mice using an acrylic anesthesia distributor (the Octamouse), with the dopamine $D_{2/3}$ ligand ^{18}F -fallypride serving as a test substance for brain receptor imaging. **Methods:** The effect of scatter correction on the small-animal PET recordings was first evaluated in phantom studies in which sources of different radioactivity concentration were placed within the chambers of the Octamouse. Next, potential effects of mass on the ^{18}F -fallypride binding potential (BP_{ND}) in the striatum were tested in groups of mice receiving ^{18}F -fallypride at 2 different specific activities (140 and 50 $\text{GBq}/\mu\text{mol}$), with and without scatter correction. Finally, the relationship between BP_{ND} and injected dose of ^{18}F -fallypride (3.5–17 MBq/mouse) was tested. **Results:** Scatter correction improved the contrast between sources and air space within the Octamouse phantom. The magnitude of ^{18}F -fallypride BP_{ND} in mouse striatum was invariant across the tested range of specific activities, and scatter correction increased BP_{ND} by a mean of 6%; covariances of the inter- and intraoperator variability of BP_{ND} were 10%. There was a positive correlation between radiochemical dose and BP_{ND} with ($R^2 = 0.53$) and without ($R^2 = 0.63$) scatter correction, which was driven by increasing area under the percentage injected dose curve in the striatum. **Conclusion:** The quantitation of emission sources placed within the Octamouse is linear over a wide range of source activities. In the striatum of living mice, the magnitude of ^{18}F -fallypride BP_{ND} was highly reproducible between operators and was constant over a 3-fold range of specific activities, indicating a lack of significant occupancy. Scatter correction improved quantitation but did not entirely correct for the dependence of BP_{ND} on injected dose, which was deemed to arise because of effects propagating from detector dead time when the total radiochemical dose in the field of view exceeded 50 MBq . Given this consideration, we were still able to quantify ^{18}F -fallypride BP_{ND} in 16 mice from a single radiosynthesis, an economy that should be generalizable to brain studies of diverse radioligands.

Key Words: Octamouse holder; dopamine $D_{2/3}$ receptor; fallypride; small-animal PET; mouse brain

J Nucl Med 2010; 51:1576–1583

DOI: 10.2967/jnumed.110.078451

Preclinical small-animal PET studies with short-lived radiotracers can entail an inefficient use of scanning resources when only a few acquisitions are obtained from a single radiosynthesis. This inefficiency is especially the case for radiotracers requiring prolonged acquisitions, such as the dopamine $D_{2/3}$ receptor ligand ^{18}F -fallypride, for which 120-min emission recordings enable a stable estimation of the binding potential (BP_{ND}) in mice. Thus, we have previously conducted small-animal PET studies of the pharmacologic modulation of ^{18}F -fallypride BP_{ND} in mouse striatum (1,2), obtaining from each radiosynthesis recordings from a mean of 5 animals. In our experience, statistical variability of the endpoint is such that a minimum group size of approximately 8 animals is necessary for detecting 20% changes in the magnitude of ^{18}F -fallypride BP_{ND} and likewise for the binding of the serotonin 5-hydroxytryptamine_{1A} antagonist ^{18}F -MPPF (3). Indeed, other researchers have used head-to-head small-animal PET recordings in pairs of rats (4) or as many as 4 simultaneous recordings for mice (5). For efficiency and to reduce the variability of the binding estimates, we consequently developed an anesthesia distributor equipped with 8 acrylic chambers (Octamouse), with external dimensions suitable for placement within the field of view of the Inveon DPET (Preclinical Solutions, Siemens Healthcare Molecular Imaging).

In the present study, we validated the use of the Octamouse for efficiently obtaining brain emission recordings from up to 16 mice from a single ^{18}F -fallypride radiosynthesis. Because counting artifacts arising from acrylic components surrounding the mice may influence the quantitation of brain signals, and thus interfere with the reliable estimation of BP_{ND} , we first conducted phantom studies in which the detector response was tested for a wide range of source radioactivities placed within the chambers of the Octamouse. We then tested the effects of scatter correction on quantitation. Next, we tested the effects of scatter cor-

Received Apr. 26, 2010; revision accepted Jul. 14, 2010.

For correspondence or reprints contact: Axel Rominger, Department of Nuclear Medicine, Ludwig-Maximilians University, Marchioninistrasse 15, 81377 Munich, Germany.

E-mail: axel.rominger@med.uni-muenchen.de

COPYRIGHT © 2010 by the Society of Nuclear Medicine, Inc.

rection on the estimation of ^{18}F -fallypride BP_{ND} in the striatum of living mice. In addition, we also tested for potential mass effects due to afternoon use of ^{18}F -fallypride obtained from a morning synthesis, during which time the specific activity decreased 3-fold. The inter- and intraoperator variabilities of our BP_{ND} estimates were assessed. Finally, we tested the dependence of BP_{ND} on the ^{18}F -fallypride radiochemical dose in the range of 3.5–17 MBq/mouse.

MATERIALS AND METHODS

Octamouse

The Octamouse is constructed from acrylic, with groups of 4 cylindrical chambers on either side of a central distributor for anesthesia gas; each cylinder has an internal diameter of 2.5 cm and accommodates mice weighing up to 22 g. The entire apparatus weighs 320 g and measures $16 \times 7 \times 7$ cm (Fig. 1A), thus fitting within the field of view of an Inveon DPET scanner.

Phantom Studies

For an initial validation of the Octamouse, we performed a phantom study using 1-mL plastic syringes (internal diameter, 4.8 mm) filled with aqueous solutions containing ^{18}F at concentrations of 2.1, 0.6, 0.18, 0.05, and 0.014 MBq/mL. Pairs of tubes of differing radioactivity were placed in each of the 8 chambers of the Octamouse, which was then positioned in the center of the field of view of the tomograph. To construct a transmission image of the Octamouse, we obtained a 30-min single-frame emission scan, followed by a 7-min transmission scan with a rotating ^{57}Co point source for attenuation correction, and finally a 30-min transmission scan.

Animal Studies

All experiments with animals were performed in compliance with the Law on Animal Experimentation of Germany. Thirty-two female BALB/c mice (mean weight \pm SD, 20.2 ± 1.6 g) purchased from Charles River Laboratories were housed in a temperature- and humidity-controlled room with a 12-h light–dark cycle, with free access to food and water.

Radiochemistry

^{18}F -fallypride was synthesized using a SynChrom R&D automatic synthesis module (Raytest Isotopenmessgeräte), as previously described (2,6).

Small-Animal PET Mouse Recordings

Anesthesia was induced with 2.5% isoflurane administered in an acrylic container and was maintained throughout the small-animal PET recordings with 1.5% isoflurane, delivered at 1.5 L/min via the central distributor of the Octamouse. After cannulation in a tail vein, groups of 8 mice were positioned within the Octamouse, which was then placed within the aperture of the Siemens Inveon DPET. Dynamic emissions lasting 120 min were initiated on serial intravenous slow-bolus injections of ^{18}F -fallypride (3.5–17 MBq) in 200 μL of saline, followed by a transmission scan using a rotating ^{57}Co point source, as previously described (2). In practice, we performed nearly simultaneous injections of 4 mice by holding 2 syringes in each hand. After a pause of 30 s (to gain access to the other side of small-animal PET scanner), we repeated the procedure and deleted the first 30-s frame in the subsequent analysis of the second group of 4 mice.

Effect of Specific Activity

To elucidate a potential effect of ^{18}F -fallypride specific activity on our BP_{ND} results, we made morning and afternoon small-animal PET recordings from a single radiosynthesis.

Inter- and Intraoperator Variability

To test the interobserver reliability of the BP_{ND} estimates, the data analysis procedure was repeated in a group of 14 animals (6 high and 8 low specific activity) by a second operator. Intraoperator variability was assessed through a reanalysis by the first operator at 2 wk after the initial analysis. Inter- and intraobserver variability was calculated for each individual mouse as follows:

$$\frac{|X1 - X2|}{(X1 + X2)/2} \times 100\%.$$

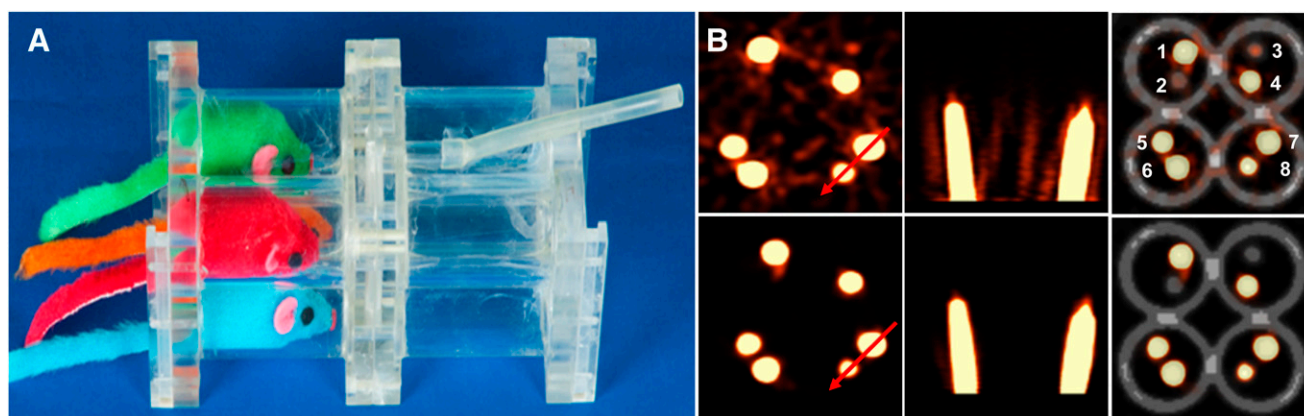


FIGURE 1. Octamouse (A) and reconstructed images (B) from phantom study without (upper row) and with (lower row) scatter-correction algorithm. Red arrows indicate position of line profiles shown in Figure 2A. From left to right are depicted coronal plane through syringes, horizontal plane, and fused PET–transmission image of source syringes within Octamouse. White numerals from 1 to 8 indicate chambers containing the following ^{18}F concentrations: 1, 2.1 MBq/mL; 2, 0.014 MBq/mL; 3, 0.05 MBq/mL; 4, 2.1 MBq/mL; 5, 0.6 MBq/mL; 6, 2.1 MBq/mL; 7, 2.1 MBq/mL; and 8, 0.18 MBq/mL.

Effect of Injected Activity

To optimize the radiochemical dose for ^{18}F -fallypride BP_{ND} estimates, we performed multiple experiments using doses ranging from 3.5 to 17 MBq of ^{18}F -fallypride, always in 200 μL of saline.

Image Reconstruction and Analysis

Phantom. Emission and transmission data were rebinned to sinograms, and scatter sinograms were produced using Siemens software, based on a standard approach (7). Sinograms were reconstructed using a combined reconstruction algorithm with two 3-dimensional ordered-subset expectation maximization iterations (Siemens Medical Solutions), followed by eighteen 3-dimensional maximum a posteriori iterations with a zoom factor of 1.0 and attenuation correction with and without scatter correction. The final result was a $128 \times 128 \times 159$ matrix, with voxel dimensions of $0.86 \times 0.86 \times 0.80$ mm.

Cylindric volumes of interest (VOIs) were positioned within the bores of the syringes. Decay- and attenuation-corrected mean radioactivity concentrations were measured within the VOIs and calculated relative to the true radioactivity concentrations of the solutions, which were measured in a calibrated γ -counter (Packard Cobra). Finally, line profiles were measured transecting the apparatus (Fig. 1B) and passing through adjacent pairs of syringes (Fig. 2A), with and without scatter correction.

Mouse Recordings

List-mode data were rebinned to sinograms, consisting of frames increasing systematically from 30 s to 10 min, for a total of 20 frames, and scatter sinograms were produced using Siemens software, based on a standard approach (7). Sinograms were reconstructed as described for the phantom study. In the specific activity study, a zoom factor of 1.3 was also used, but without scatter correction, resulting in voxel dimensions of $0.66 \times 0.66 \times 0.80$ mm. The small-animal PET files were converted to NIFTI data format via PMOD software (PMOD Technologies Ltd.). The summation images were calculated for each dynamic ^{18}F -fallypride recording, converted to Montreal Neurological Institute format (MNI), and manually coregistered to a digital MRI volume atlas of the mouse brain (8) using Register-1.3.6 and Minc-2.0.9 software (MNI-BIC Software). Registration was accomplished using rigid-body transformation with 9° of freedom, as described previously (2). Then, the 120-min dynamic ^{18}F -fallypride images were resampled to the common space; the absence of substantial head movement was verified by frame-by-frame examination of the resampled dynamic images. After transformation back to NIFTI format, images were processed further using the PMOD software. Voxelwise parametric maps of the binding potential ($BP_{ND} \approx k_3/k_4$) were calculated using linear graphical analysis

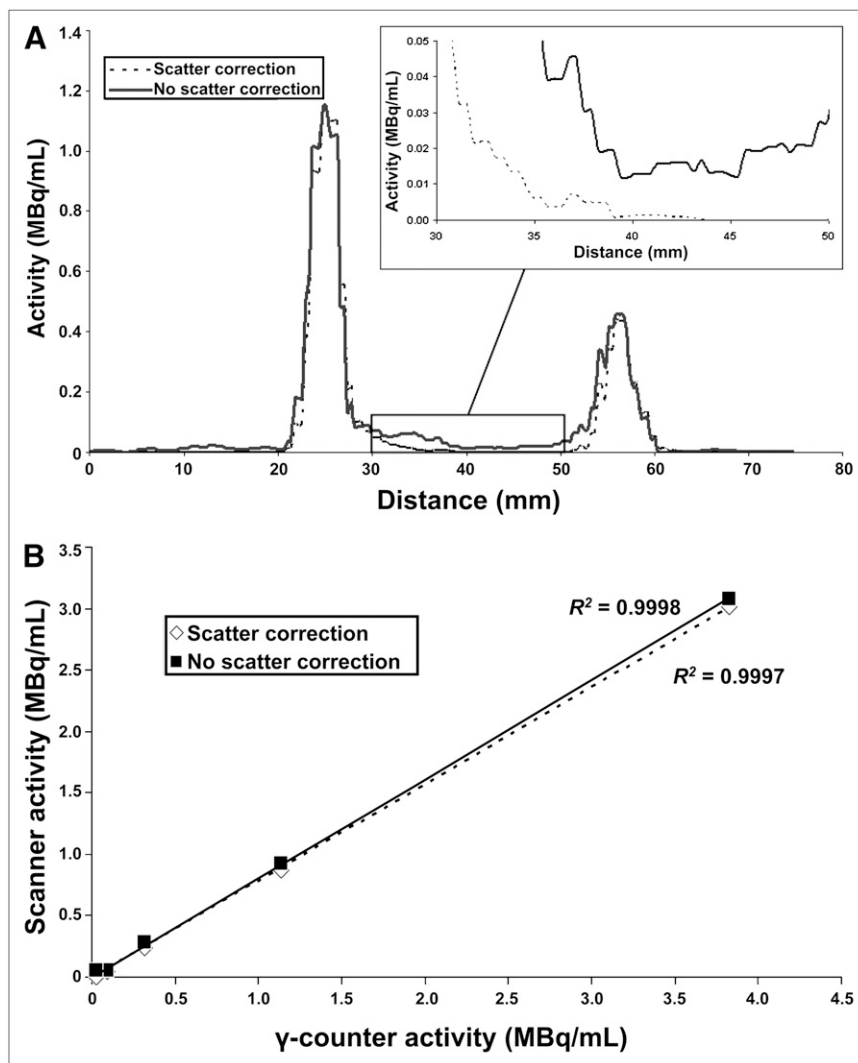


FIGURE 2. (A) Line profiles of syringe sources with and without scatter-corrected reconstructions. Inset shows magnification of one of the voids between syringes, indicating that scatter correction reduced measurements toward true zero background. (B) Corresponding linear relationship between source radioactivity concentrations measured in calibrated γ -counter and measured by small-animal PET.

TABLE 1. Inter- and Intraoperator Variability and Impact of Zoom Factor and Scatter Correction

Striatal BP_{ND} ...	High specific activity ($n = 6$)	Low specific activity ($n = 8$)	P (high vs. low specific activity)
Without scatter correction, zoom of 1.3	6.73 ± 0.93	6.45 ± 0.78	NS
Without scatter correction, zoom of 1.0	5.75 ± 0.82	5.65 ± 0.76	NS
	$P < 0.01$ (vs. zoom of 1.3)	$P < 0.01$ (vs. zoom of 1.3)	
With scatter correction, zoom of 1.0	6.10 ± 0.87	6.00 ± 0.80	NS
	$P < 0.001$ (vs. no scatter correction)	$P < 0.001$ (vs. no scatter correction)	
Intraoperator, without scatter correction, zoom of 1.0	5.84 ± 0.58	5.49 ± 0.34	NS
Interoperator, without scatter correction, zoom of 1.0	6.09 ± 0.47	5.65 ± 0.58	NS
Mean MBq	6.30 ± 0.28	5.67 ± 0.41	NS

NS = not significant.
Data are mean \pm SD.

(9), with a reference tissue input derived from a 0.8-mm-diameter spheric VOI placed within the cerebellum. Mean BP_{ND} maps were calculated by group for each condition and were resampled into the common stereotactic space. Mean magnitudes of the voxelwise estimates of BP_{ND} were calculated for the left and right striatum, using spheric VOIs as described previously (2). An asymmetry index ($[\text{left} - \text{right}]/[\text{left} + \text{right}]$) was calculated for the striatum, as described in humans (10). Because no asymmetry (1.4%, not significant) was observed in the group of 32 mice, the left and right striatal VOIs were combined. In the specific activity experiment ($n = 14$), we also placed a spheric VOI on the petrosal bone.

Statistical Analysis

Results were reported as the mean value and SD. Unpaired t tests were used in the comparisons of the different groups.

RESULTS

Phantom Results

Figure 1B shows emission recordings with syringes containing 0.014–2.1 MBq of ^{18}F -fluoride superimposed on a transmission scan of the Octamouse. Line profiles passing through several syringes of different radioactivity concentrations show that, without scatter correction, the trough activities in the air spaces are overestimated (Fig. 2A).

Figure 2B shows that small-animal PET concentration measurements recorded from cylindric sources with a 4.8-mm internal diameter (i.e., twice the full width at half maximum for the reconstructed images) had a nearly perfect correlation between PET and γ -counter measurements over the entire concentration range. The efficiency of small-animal PET was 82% and nearly identical with and without scatter correction.

Mouse Results

Issues of Specific Activity, Scatter Correction, Observer Variability, and Zoom Factor. In the specific activity study, morning mice received a mean dose of 6.2 ± 0.8 MBq of specific activity (140 GBq/ μmol), whereas afternoon mice

received a mean dose of 5.8 ± 0.7 MBq (not significant) of specific activity (50 GBq/ μmol). The mean striatal BP_{ND} was invariant with specific activity (Table 1). Compared with a zoom factor of 1.3, a lower zoom factor of 1.0, as required if the transmission recording is to encompass the entire Octamouse, resulted in a 15% underestimation of striatal BP_{ND} . For the subgroup of 14 mice receiving 5.8–6.5 MBq of ^{18}F -fallypride, scatter correction led to a highly significant 6% increase of BP_{ND} . For this same subgroup, interobserver variance was 11.2%, and intraobserver variance was 8.6%. Figure 3 shows the corresponding mean parametric images for zoom factors 1.3 and 1.0 without scatter correction and for zoom factor 1.0 with scatter correction in 3 planes projected on the mouse brain MRI atlas.

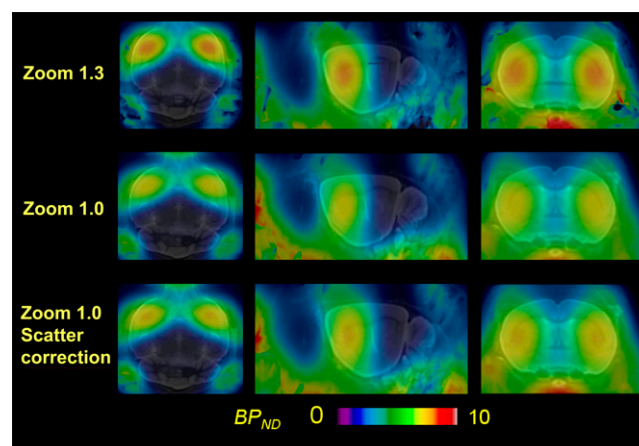


FIGURE 3. Mean parametric maps of ^{18}F -fallypride BP_{ND} projected on MRI mouse atlas (gray scale) in horizontal, left sagittal, and coronal planes of mice with different zoom factors and with or without scatter correction. The mean injected dose (\pm SD) was 5.9 ± 0.5 MBq ($n = 14$).

Effect of Injected Radioactivity on BP_{ND}

The magnitude of BP_{ND} correlated with the individual amount of injected radioactivity for all 32 mice analyzed with a zoom factor of 1.0; application of the scatter correction decreased the linear regression slope (Figs. 4A and 4B). Figure 5A shows the mean time–activity curves in the striatum, cerebellum, and petrosal bone from the 8 mice with the lowest injected radioactivity (range, 3.4–5.5 MBq; mean, 4.7 MBq). Figure 5B shows the corresponding curves from the 8 mice with the highest dose of injected radioactivity (range, 9.5–17.1 MBq; mean, 12.7 MBq); also depicted are the corresponding mean parametric maps in a representative axial slice passing through the striatum. The area under the curve (AUC) of the striatal time–activity curves were significantly lower in the group with low radiochemical dose (712 ± 107) than in the group with high dose (847 ± 131 ; $P < 0.04$), whereas the corresponding cerebellum AUCs did not differ (153 ± 40.3 vs. 144 ± 29.6 ; not significant), nor did the petrosal bone recording AUCs (241 ± 23.2 vs. 261 ± 58.3 ; not significant).

DISCUSSION

The goal of this study was to establish and validate the use of the Octamouse, an acrylic insert for simultaneous small-animal PET scanning of 8 isoflurane-anesthetized mice, to optimize the yield of data acquisition from a single radiosynthesis. We first conducted phantom studies to assess scatter effects arising from the Octamouse on the quantitation of sources placed within the chambers and

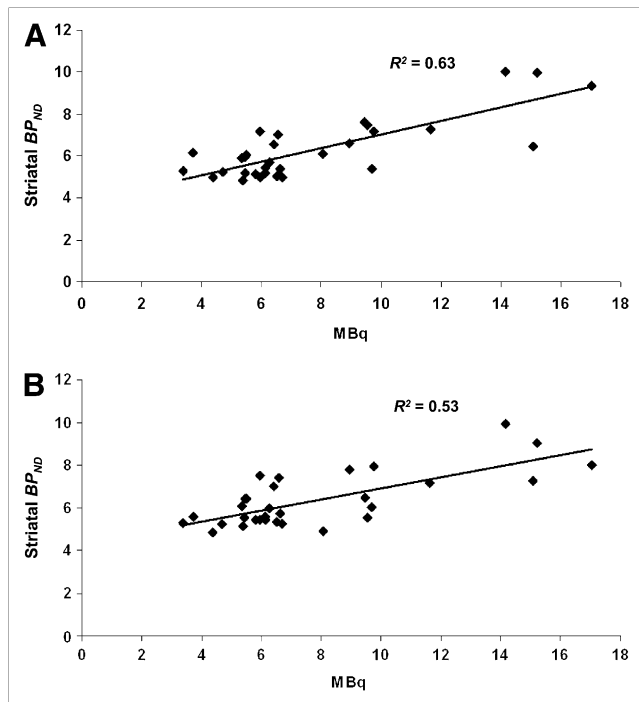


FIGURE 4. Correlation of ^{18}F -fallypride BP_{ND} with amount of injected activity (MBq) without (A) and with (B) scatter correction ($n = 32$) in mouse striatum.

systematically investigated the contributions of several postprocessing steps on the quantitation of ^{18}F -fallypride binding to dopamine $D_{2/3}$ receptors in the striatum of living mice. There have hitherto been few reports describing a multichamber approach for small-animal PET recordings. One study has described an insert for simultaneous nose-to-nose scanning of 2 rats (4). Inserts have also been used for obtaining precise repositioning of animals in serial PET studies or multimodal imaging studies of rats (11) and also mice (12). Simultaneous small-animal PET recordings have been obtained in as many as 4 mice (5). However, this is the first report, to our knowledge, on the use of a multichamber holder for the scanning of 8 mice, and at least 16 mice from a single radiosynthesis. Although the use of an acrylic insert presents a clear advantage in economy, especially when large groups and long dynamic acquisitions are required, several technical issues relevant to quantitation are raised.

The phantom studies showed linear response of the small-animal PET scanner for a wide range of source radio-

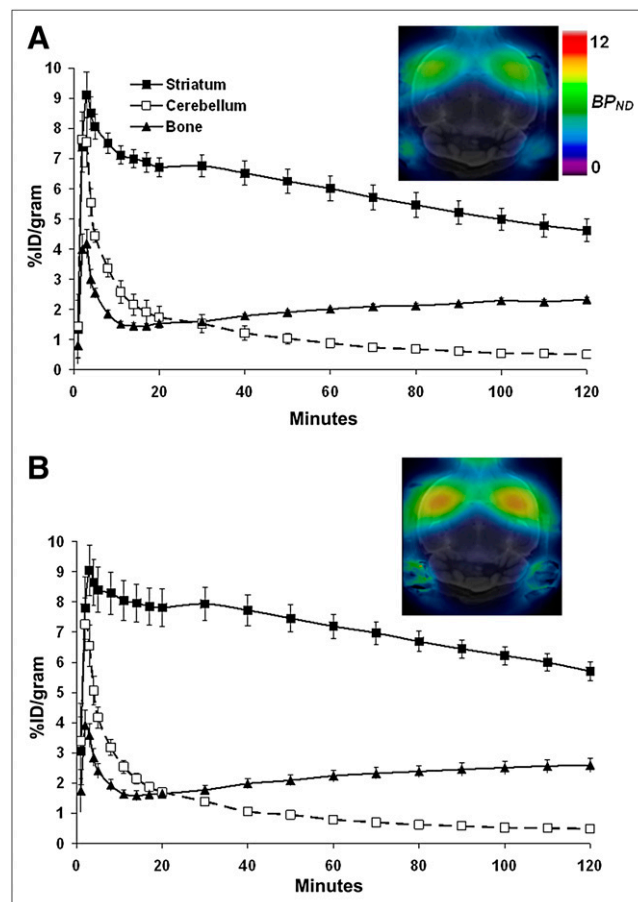


FIGURE 5. Mean (\pm SEM) time–activity curves in striatum, cerebellum, and petrosal bone of groups of 8 mice with low ^{18}F -fallypride dose (4.7 ± 0.8 MBq) (A) and high ^{18}F -fallypride dose (12.7 ± 3.0 MBq) (B). Inserts show corresponding mean parametric maps of ^{18}F -fallypride BP_{ND} in axial plane passing through striatum. %ID = percentage injected dose.

activities placed within the Octamouse chambers. Counting efficiency was close to 82%, as expected from the geometry of cylindrical sources with diameters twice the full width at half maximum of the small-animal PET scanner. However, the phantom images revealed the presence of considerable radioactivity throughout the air spaces of the chambers, which we attributed to scatter from the relatively massive Octamouse. Indeed, application of a standard scatter-correction algorithm substantially improved the image quality (Fig. 1B). The line profiles placed across the sources indicated that scatter correction decreased the trough activities toward the true background activity, which propagated to a 6% increase in ^{18}F -fallypride BP_{ND} . This effect was highly significant, because it occurred in almost every animal. Thus, scatter is an avoidable source of bias in the quantitation of signals arising from within the Octamouse.

We have previously characterized the binding of ^{18}F -fallypride in the striatum of mice scanned in groups of 2–4 animals without an acrylic holder (1,2). In those studies, we used a zoom factor of 1.3 to restrict the reconstructed volume, which led to a decreased voxel size and, consequently, fewer partial-volume effects, in turn propagating a somewhat higher BP_{ND} . However, because the 1.3 zoom factor does not encompass the entire Octamouse, the attenuation and scatter correction would not properly account for mass outside the field of view. Lowering the zoom factor to 1.0 resulted in a more accurate attenuation correction throughout the field of view of the small-animal PET scanner but reduced the apparent magnitude of ^{18}F -fallypride BP_{ND} by 14% (Table 1; Fig. 3).

Mass effects can potentially influence the outcome measure in small-animal PET studies with ^{18}F -fallypride and other tracers. We have earlier shown by calculation that the occupancy of dopamine $D_{2/3}$ receptors is less than 5% in mice receiving 10 MBq of ^{18}F -fallypride (2). In the present study, we made a more systematic test of possible mass effects by comparing BP_{ND} estimates in groups of mice, with ^{18}F -fallypride specific activity declining by a factor of 3; we found no associated decline in specific binding, indicating a lack of mass effects within the range of specific activity (140–50 GBq/ μmol) encountered in our laboratory. Much more problematic with respect to small-animal PET quantitation is the difficulty in obtaining adequate spatial normalization for objects as small as the mouse brain. This should be remedied in the future, with the advent of hybrid small-animal PET/CT and small-animal PET/MRI but remains for the present a manual task requiring considerable skill and practice. Because BP_{ND} estimates are highly vulnerable to the misplacement of the VOIs, especially for the reference region, the manual registration is a potential source of experimental error or bias. However, our inter- and intraoperator covariances in the estimation of ^{18}F -fallypride BP_{ND} (10%) were of the same scale as the variance with a subpopulation of 14 mice, indicating that skillful operators can obtain adequately reproducible quantitation.

In our earlier ^{18}F -fallypride small-animal PET studies, we found a mean striatal BP_{ND} of 10 in saline-treated mice; these animals, scanned in groups of 2–4 with a zoom factor of 1.3, had all received a radiochemical dose of 10 MBq of ^{18}F -fallypride. In the course of the present specific activity study with 14 mice, we administered only 6 MBq of ^{18}F -fallypride and found a mean BP_{ND} of only 6. For the entire present population of 32 mice, there was a highly significant positive correlation between the injected dose and BP_{ND} . Because the magnitude of BP_{ND} is, in general, a steady-state ratio between the high binding and reference region activities, there is no a priori reason to expect dose effects, so long as receptor occupancy is minimal. Because mass effects are excluded, we had to find an alternative explanation for this unexpected phenomenon. Initial considerations focused on the potentially biasing effects of spill-in from the cranium, which can be quite significant at late ^{18}F -fallypride circulation times (2). Defluorination of certain gaseous anesthetics in rodent liver microsomes proceeds as a zero-order process (13,14), which might have predicted mass effects on the rate of accumulation in bone of ^{18}F -fluoride derived from the hepatic metabolism of ^{18}F -fallypride. However, the time–activity curves from the petrosal bone did not reveal any differential labeling as a function of specific activity.

The relatively heavy acrylic holder is a source of scatter, which biased BP_{ND} estimates, as noted in the “Discussion” section. The application of a scatter-correction algorithm attenuated by 20% the slope of the relationship between individual injected dose and apparent BP_{ND} . The remaining 80% of the correlation must arise from other factors, because the scatter-corrected striatal AUC in the high-dose mice exceeded that in the low-dose mice, whereas the mean cerebellum AUCs did not significantly differ, and the petrosal uptake had only a trend toward increased signal (Fig. 5). Using a rat-sized phantom in the Inveon DPET scanner, Kemp et al. found an increasing mean relative counting rate error with increasing radioactivity (15), especially when the total radioactivity in the field of view exceeded 74 MBq for a rat-sized phantom. Given that the Octamouse is larger than the rat phantom, we can predict that the cutoff value should be lower, perhaps 50 MBq.

When total radioactivity in the field of view exceeds a certain limit, dead-time correction (which is applied globally) alters the contrast between regions of high and low radioactivity, thus plausibly accounting for the increase in apparent BP_{ND} . Indeed, our experiments with 10 MBq per mouse resulted in total activity as high as 80 MBq within the Octamouse. To avoid faulty dead-time correction, future Octamouse studies will be limited to a total of 40 MBq (8×5 MBq), this change having the additional advantage of reducing the maximum required injection volume to 160 μL per mouse.

We have considered some of the many possible sources of error and bias in BP_{ND} estimation by small-animal PET.

In addition, it must be considered that the linear graphical Logan analysis used in the present study (9) is inherently vulnerable to noise effects, which led, in our hands, to underestimated voxelwise maps of ^{11}C -raclopride BP_{ND} in the pig brain (16) and ^{18}F -MPPF BP_{ND} in the rat brain (3). Quantitation of ^{18}F -fallypride BP_{ND} in mice is vulnerable to effects with opposing biases, perhaps none so important as the effects of partial volume; the size of the mouse striatum (50 mm^3) is such that small-animal PET estimates of ^{18}F -fallypride BP_{ND} are less than half of the true value obtained by dissection of the mouse brain *ex vivo* (2). In the 2 earlier mouse small-animal PET studies with ^{18}F -fallypride, the BP_{ND} estimates were 13 (17) and 3.2 (18); this difference likely reflects the high resolution of the quad-HIDAC PET (17) used by Honer et al. ($<1\text{ mm}$), and the relatively lower resolution of the Advanced Technology Laboratory Animal Scanner (National Institutes of Health) and Siemens Focus 120 scanner used by Skinbjerg et al. (1.6 mm) (18). Rat small-animal PET studies found ^{18}F -fallypride BP_{ND} of 7 (19) and 8 (20), or a striatum-to-cerebellum ratio of 8 (21), whereas Tantawy et al., using a full-compartmental analysis of 2-h dynamic recordings, found a BP_{ND} in rat striatum of 13 (22). Thus, the increment in striatal volume between rats and mice does not seem to consistently result in improved quantitation of BP_{ND} , although a direct comparison of mouse and rat has not yet been made.

Whereas monkey PET studies found striatum-to-cerebellum ratios ranging from 3 to 9, depending on the time frame (6,21,23), prolonged recordings ^{18}F -fallypride gave BP_{ND} estimates of 27 (24) and 23 (25). Thus, results in the monkey compare well with those in the human brain (26–28), as expected for the primate striatum, which is 10- to 20-fold larger than in rodents. Disregarding the possible attainment of submillimeter small-animal PET resolution, more accurate BP_{ND} estimates in mouse striatum might be obtainable through the use of a partial-volume correction (29).

CONCLUSION

The Octamouse enables the efficient use of ^{18}F -fallypride from a single radiosynthesis, making the Octamouse a favorable device for conducting dose–response studies of pharmacologic challenges in relatively large groups of animals. The results of our study should be generalizable for small-animal PET studies with diverse neuroreceptor ligands. The next version of the Octamouse accommodates mice weighing 35 g, as will be required for longitudinal and transgenic studies.

ACKNOWLEDGMENTS

We thank Georg Stark for technical assistance with the construction of the Octamouse and Cornelia Arszol for technical assistance. This project was supported by a grant of the Medical Faculty of the University of Munich (FöFoLe).

REFERENCES

- Rominger A, Mille E, Boning G, et al. α_2 -Adrenergic drugs modulate the binding of [^{18}F]fallypride to dopamine $D_{2/3}$ receptors in striatum of living mouse. *Synapse*. 2010;64:654–657.
- Rominger A, Wagner E, Mille E, et al. Endogenous competition against binding of [^{18}F]DMFP and [^{18}F]fallypride to dopamine $D_{2/3}$ receptors in brain of living mouse. *Synapse*. 2010;64:313–322.
- la Fougere C, Boning G, Bartmann H, et al. Uptake and binding of the serotonin 5-HT1A antagonist [^{18}F]MPPF in brain of rats: effects of the novel P-glycoprotein inhibitor tariquidar. *Neuroimage*. 2010;49:1406–1415.
- Cheng TE, Yoder KK, Normandin MD, et al. A rat head holder for simultaneous scanning of two rats in small animal PET scanners: design, construction, feasibility testing and kinetic validation. *J Neurosci Methods*. 2009;176:24–33.
- Skinbjerg M. *Dopamine D2 Receptor Pharmacology: In Vitro Analyses and In Vivo PET Imaging* [Ph.D. dissertation]. Stockholm, Sweden: Karolinska Institute; 2009.
- Mukherjee J, Yang ZY, Das MK, Brown T. Fluorinated benzamide neuroleptics. III. Development of (*S*)-*N*-[(1-allyl-2-pyrrolidinyl)methyl]-5-(3-[^{18}F]fluoropropyl)-2,3-dimethoxybenzamide as an improved dopamine D-2 receptor tracer. *Nucl Med Biol*. 1995;22:283–296.
- Watson CC. New, faster, image-based scatter correction for 3D PET. *IEEE Trans Nucl Sci*. 2000;47:1587–1594.
- Dorr A, Sled JG, Kabani N. Three-dimensional cerebral vasculature of the CBA mouse brain: a magnetic resonance imaging and micro computed tomography study. *Neuroimage*. 2007;35:1409–1423.
- Logan J, Fowler JS, Volkow ND, Wang GJ, Ding YS, Alexoff DL. Distribution volume ratios without blood sampling from graphical analysis of PET data. *J Cereb Blood Flow Metab*. 1996;16:834–840.
- Vernaleken I, Weibrich C, Siessmeier T, et al. Asymmetry in dopamine $D_{2/3}$ receptors of caudate nucleus is lost with age. *Neuroimage*. 2007;34:870–878.
- Rubins DJ, Meadors AK, Yee S, Melega WP, Cherry SR. Evaluation of a stereotactic frame for repositioning of the rat brain in serial positron emission tomography imaging studies. *J Neurosci Methods*. 2001;107:63–70.
- Suckow C, Kuntner C, Chow P, Silverman R, Chatziioannou A, Stout D. Multimodality rodent imaging chambers for use under barrier conditions with gas anesthesia. *Mol Imaging Biol*. 2009;11:100–106.
- Rice SA, Sbordone L, Mazze RI. Metabolism by rat hepatic microsomes of fluorinated ether anesthetics following isoniazid administration. *Anesthesiology*. 1980;53:489–493.
- Burke TR Jr., Martin JL, George JW, Pohl LR. Investigation of the mechanism of defluorination of enflurane in rat liver microsomes with specifically deuterated derivatives. *Biochem Pharmacol*. 1980;29:1623–1626.
- Kemp BJ, Hruska CB, McFarland AR, Lenox MW, Lowe VJ. NEMA NU 2-2007 performance measurements of the Siemens Inveon preclinical small animal PET system. *Phys Med Biol*. 2009;54:2359–2376.
- Cumming P, Rosa-Neto P, Watanabe H, et al. Effects of acute nicotine on hemodynamics and binding of [^{11}C]raclopride to dopamine $D_{2,3}$ receptors in pig brain. *Neuroimage*. 2003;19:1127–1136.
- Honer M, Bruhlmeier M, Missimer J, Schubiger AP, Ametamey SM. Dynamic imaging of striatal D_2 receptors in mice using quad-HIDAC PET. *J Nucl Med*. 2004;45:464–470.
- Skinbjerg M, Liow JS, Seneca N, et al. D_2 dopamine receptor internalization prolongs the decrease of radioligand binding after amphetamine: a PET study in a receptor internalization-deficient mouse model. *Neuroimage*. 2010;50:1402–1407.
- Dalley JW, Fryer TD, Brichtard L, et al. Nucleus accumbens $D_{2/3}$ receptors predict trait impulsivity and cocaine reinforcement. *Science*. 2007;315:1267–1270.
- Yakushev IY, Dupont E, Buchholz HG, et al. In vivo imaging of dopamine receptors in a model of temporal lobe epilepsy. *Epilepsia*. 2010;51:415–422.
- Mukherjee J, Yang ZY, Brown T, et al. Preliminary assessment of extrastriatal dopamine D-2 receptor binding in the rodent and nonhuman primate brains using the high affinity radioligand, ^{18}F -fallypride. *Nucl Med Biol*. 1999;26:519–527.
- Tantawy MN, Jones CK, Baldwin RM, et al. [^{18}F]Fallypride dopamine D_2 receptor studies using delayed microPET scans and a modified Logan plot. *Nucl Med Biol*. 2009;36:931–940.
- Mukherjee J, Yang ZY, Lew R, et al. Evaluation of d-amphetamine effects on the binding of dopamine D-2 receptor radioligand, ^{18}F -fallypride in

- nonhuman primates using positron emission tomography. *Synapse*. 1997; 27:1–13.
24. Christian BT, Narayanan T, Shi B, Morris ED, Mantil J, Mukherjee J. Measuring the in vivo binding parameters of [¹⁸F]-fallypride in monkeys using a PET multiple-injection protocol. *J Cereb Blood Flow Metab*. 2004;24:309–322.
25. Slifstein M, Hwang DR, Huang Y, et al. In vivo affinity of [¹⁸F]fallypride for striatal and extrastriatal dopamine D2 receptors in nonhuman primates. *Psychopharmacology (Berl)*. 2004;175:274–286.
26. Cropley VL, Innis RB, Nathan PJ, et al. Small effect of dopamine release and no effect of dopamine depletion on [¹⁸F]fallypride binding in healthy humans. *Synapse*. 2008;62:399–408.
27. Mukherjee J, Christian BT, Dunigan KA, et al. Brain imaging of ¹⁸F-fallypride in normal volunteers: blood analysis, distribution, test-retest studies, and preliminary assessment of sensitivity to aging effects on dopamine D-2/D-3 receptors. *Synapse*. 2002;46:170–188.
28. Lee B, London ED, Poldrack RA, et al. Striatal dopamine D₂/D₃ receptor availability is reduced in methamphetamine dependence and is linked to impulsivity. *J Neurosci*. 2009;29:14734–14740.
29. Rousset OG, Deep P, Kuwabara H, Evans AC, Gjedde AH, Cumming P. Effect of partial volume correction on estimates of the influx and cerebral metabolism of 6-[¹⁸F]fluoro-L-dopa studied with PET in normal control and Parkinson's disease subjects. *Synapse*. 2000;37:81–89.